

A SHARP DIFFUSE-INTERFACE APPROACH TO COMPRESSIBLE MULTI-FLUID FLOWS

CHAO ZHANG¹ AND IGOR MENSHOV^{1,2,3}

¹ MSU, Faculty of Mechanics and Mathematics
GSP-1, 1 Leninskiye Gory, 119991, Moscow, Russia
zhang-c@mail.ru

² Keldysh Institute for Applied Mathematics RAS
Miusskaya sq, 4, 125047, Moscow, Russia
menshov@kiam.ru

³ VNIIA, ROSATOM CORP.
st. Sushchevskaya, 22, 127055, Moscow, Russia
imen57@mail.ru

Key words: Multi-Fluid Dynamics, Diffuse-Interface Methods, Eulerian Grids.

Abstract. A numerical approach for modeling heterogeneous media composed of multiple compressible materials with different physical properties is considered. The model is single-velocity, and the governing equations represent mass conservation for each component, conservation of the total momentum and energy, and advection of $N-1$ characteristic functions that depend on volume fractions of N components. The isobaric assumption is used to close the model equations. We consider the second-order accurate Godunov-type numerical scheme for solving the system of governing equations. It is shown that for meeting the PV and monotonicity properties of the numerical solutions, different characteristic functions should be taken for the advection operator and for the face-interpolator, and such functions are proposed. We test the proposed model and numerical method with several benchmark problems. The results obtained show that the method is robust and effective in capturing interfaces in multimaterial compressible hydrodynamics, providing non-oscillatory and physically admissible solutions.

1 INTRODUCTION

We consider hydrodynamics of a heterogeneous continuum medium that consists of N materials (components) separated by sharp interfaces. The components are compressible ideal fluids with different equation of states. The mathematical model describing such multi-fluid flows consists of the compressible Euler equations closed by the equation of state that change the functional form or control parameters when we cross the interface between two components. The Lagrangian approach is most appropriate for solving multi-fluid flow problems as the interfaces are tracked by grid lines, and the problem solution is naturally split into solution of a set of single-material subproblems. However, this approach is rather restrictive, and can be applied only for those problems where the deformation of the interface

is not too much.

Eulerian or Arbitrary Lagrangian-Eulerian (ALE) methods better fit problems with large interface deformation. The material interface is typically represented in these methods by volume fractions, thermodynamic parameters or level-set functions. One can distinguish two groups of methods that are referred in literature as interface-tracking and interface-capturing, respectively. In the first group (interface-tracking), the interface is explicitly calculated or restored at each time step, and its location is used in the solution procedure. Methods related to this group are: volume-of-fluid [1], moment-of-fluid [2], ALE [3], front-tracking [4], level set/ghost fluid [5] schemes, and the ghost fluid method [6]. These methods are not conservative nearby the interface and can lead to errors in its positioning.

Interface-capturing methods [7-9] introduce material-related parameters that can diffuse near the interface. These parameters can be thermodynamic parameters in the equation of state or volume fractions governed by the advection equation. The intermediate (diffused) parameters may cause spurious numerical oscillations in the solution near the interface. Also, an important property of maintaining constant pressure and velocity distributions (well-balancing property) must hold when developing an interface-capturing method for multifluid flows.

The method proposed by Allaire et al. [9] for the case of two fluids is one that meets the above requirements. It is designed to be monotone in the vicinity of the interface and meet the well-balancing condition. However, its extension to more than two components is not evident. A multiple-fluid model must ensure two conditions for the volume fractions. Namely, the volume fraction of each fluid must be in the interval $[0,1]$, and the summation of all volume fractions must equal 1. Violation of these conditions leads to unphysical numerical solutions and even code failure.

It is noted in [9] that a generalized numerical model to treat more than two fluids can be constructed by adding a partial density conservation equation and a volume fraction advection equation for each additional fluid component. Later, M.B. Friess and S. Kokh proposed a $(2N+2)$ -equation model [10], which is considered to be an extension of the baseline five-equation model [1] to the case of N ($N \geq 3$) components. Their model consists of $(2N+2)$ equations, including N conservation equations for partial densities, the conservation equation of momentum, the conservation equation of energy, and N advection equations for volume fractions. To ensure the above-mentioned two conditions for the volume fractions, recursive constructions of the trust interval of the volume fraction are implemented.

In the present work, we propose an alternative model for multi-fluid flows that is represented by the system of $(2N+1)$ -equations. Instead of directly solving the advection equation for volume fractions, we use properly chosen advection functions to update and reconstruct volume fractions so as to satisfy aforementioned constraint conditions for volume fractions. The model is proven to possess consistency of the closure model (i.e., unique recovering of primitive variables from conservative variables), hyperbolicity, and entropy condition.

2 NUMERICAL MODEL

Considering multi-fluid flow, we introduce a color function z_i , $i=1, \dots, N$ which represents the volume fraction of the component i in the mixture,

$$\sum_i^N z_i = 1, z_i \in [0,1] , \quad (1)$$

and $2N+1$ equations for mass conservation of each component, conservation of the total momentum and total energy, and advection of $N-1$ characteristic functions:

$$\begin{cases} \frac{\partial z_i \rho_i}{\partial t} + \text{div } z_i \rho_i \mathbf{u} = 0, & i = 1, 2, \dots, N, \\ \frac{\partial \rho \mathbf{u}}{\partial t} + \text{div } \rho \mathbf{u} \otimes \mathbf{u} + P \mathbf{I}_d = 0, \\ \frac{\partial \rho e}{\partial t} + \text{div } \rho H \mathbf{u} = 0, \\ \frac{\partial f_j}{\partial t} z_1, z_2, \dots, z_{N-1} + \mathbf{u} \cdot \text{grad} f_j z_1, z_2, \dots, z_{N-1} = 0, & j = 1, 2, \dots, N-1. \end{cases} \quad (2)$$

where $\rho = \sum_{i=1}^N z_i \rho_i$, $P = \sum_{i=1}^N z_i P_i$, and $\varepsilon = \frac{1}{\rho} \sum_{i=1}^N z_i \rho_i \varepsilon_i$ are the mixture density, pressure, and specific internal energy, respectively, $e = \varepsilon + 0.5 |\mathbf{u}|^2$ and $H = e + P/\rho$ are the total energy and enthalpy. The Jacobian of the advection functions with respect to the volume fractions must be non zero, $\partial f / \partial z \neq 0$.

We assume that material of each fluid is described by a generalized EOS in the following form:

$$P_i(\rho_i, \rho_i \varepsilon_i) = G_i(\rho_i, \rho_i \varepsilon_i) - H_i(\rho_i) . \quad (3)$$

with $G_i(\rho_i) > 0$. This form includes a wide range of EOS such as ideal gas, van der Waals gas, stiffened gas, Mie-Gruneisen EOS for solids.

We use the isobaric assumption $P = P_1(\rho_1, \rho_1 \varepsilon_1) = P_2(\rho_2, \rho_2 \varepsilon_2) = \dots = P_N(\rho_N, \rho_N \varepsilon_N)$ to close the system (2). One can prove that this closure model admits unique recovery of pressure P from the vector of conservative variables providing that the EOS of each component is taken in the generalized form (3).

The FVM method with the HLLC numerical flux is implemented to solve the system of equations (2). To do this, the equations for the characteristic functions in (2) are recast in a quasi-conservative form by rearranging $\mathbf{u} \cdot \text{grad} f = \text{div}(f \mathbf{u}) - f \text{div} \mathbf{u}$. The first term can be viewed as the flux term and calculated together with the conservative equations of (2) by using the HLLC numerical flux. The second (non-conservative) term is then treated as a source term and approximated in terms of the cell averaged value f and the face value $u_n = (\mathbf{u}, \mathbf{n})$, \mathbf{n} is the outward unit normal to the face.

Thus, the HLLC numerical flux for the conservative part of the system (2) is given by

$$\mathbf{F}_\sigma = \frac{1 + \text{sgn } s^*}{2} [\mathbf{F}_L + s_- \mathbf{W}_{*L} - \mathbf{W}_L] + \frac{1 - \text{sgn } s^*}{2} [\mathbf{F}_R + s_+ \mathbf{W}_{*R} - \mathbf{W}_R] \quad (4)$$

where \mathbf{W}_{*L} and \mathbf{W}_{*R} are the state vectors characterizing the states on the left and right of the intermediate contact wave, respectively,

$$\mathbf{W}_{*K} = \begin{pmatrix} \frac{s_K - u_K}{s_K - s_*} \end{pmatrix} \begin{bmatrix} z_1 \rho_{1K} \\ z_2 \rho_{2K} \\ \vdots \\ z_N \rho_{NK} \\ \rho_K s_* \\ \rho_K v_K \\ \rho_K w_K \\ \rho_K e_K + s_* - u_K \left(\rho_K s_* + \frac{P_K}{s_K - u_K} \right) \\ f_{1,K} \\ \vdots \\ f_{N-1,K} \end{bmatrix}, K = L, R. \quad (5)$$

and $s_{\mp} = \min(0, s_{L/R})$, $s_{L/R} = \min(\bar{u} \mp \bar{c}, u_{L/R} \pm c_{L/R})$ are the estimated wave velocities. The bar here means the Roe average. The speed of the contact discontinuity and the velocity in the source term (that must be consistent with the velocity used in the conservative numerical flux to hold valid the PV condition) are calculated, respectively, as

$$s_* = \frac{P_R - P_L + \rho_L u_L (s_L - u_L) - \rho_R u_R (s_R - u_R)}{\rho_L (s_L - u_L) - \rho_R (s_R - u_R)} \quad (6)$$

$$u_n = \frac{1 + \text{sgn}(s_*)}{2} \left[u_L + s_- \left(\frac{s_L - u_L}{s_L - s_*} - 1 \right) \right] + \frac{1 - \text{sgn}(s_*)}{2} \left[u_R + s_- \left(\frac{s_R - u_R}{s_R - s_*} - 1 \right) \right]. \quad (7)$$

More details regarding the HLLC numerical flux approximation can be found in [15-16].

3 CHARACTERISTIC ADVECTION FUNCTIONS

We propose to employ different advection functions for the operator of face interpolation and time step updating. The flow of more than two components is different from and more complicated than the flow of only two components. For multi-fluid flows with N ($N \geq 3$) components, if given initial conditions such that:

$$\begin{cases} z_i^0(x) \in [0, 1], & x \in [x_L, x_R], \quad i = 1, 2, \dots, N, \\ \sum_i^N z_i^0(x) = 1, & x \in [x_L, x_R], \end{cases} \quad (8)$$

the following two conditions should be ensured:

$$\begin{cases} z_i(x, t) \in [0, 1], & x, t \in [x_L, x_R] \times [0, T], \quad i = 1, 2, \dots, N, \quad T > 0, \\ \sum_i^N z_i(x, t) = 1, & x, t \in [x_L, x_R] \times [0, T], \quad T > 0. \end{cases} \quad (9)$$

or

$$\begin{cases} z_i(x, t) \in [0, 1], & x, t \in [x_L, x_R] \times [0, T], \quad i = 1, 2, \dots, N, \quad T > 0, \\ \sum_i^n z_i(x, t) < 1, & x, t \in [x_L, x_R] \times [0, T], \quad T > 0, \quad 1 \leq n \leq N-1. \end{cases} \quad (10)$$

These conditions are satisfied by the first order upwind scheme (HLLC scheme), but not by nonlinear higher order schemes such as MUSCL and WENO, if they are implemented independently to each volume fraction. In fact, when $N=2$, the two constraints are equivalent. This is different from the case of three and more components when summation of a part of the volume fractions may occur larger than 1 after evolution with time, resulting in a negative sum of the other volume fractions and inducing spurious oscillations. The root of this defect lies in that the interpolated values $z_{cf,i}$ at cell faces may violate constraint (9) or (10). Similar problem has been studied by Jaouen [11], where the conditions (9) and (10) are ensured by setting a trust interval for the numerical fluxes.

In the present paper, we deal with this problem in a different way. We propose special characteristic functions with which the constraints on volume fractions are kept after the implementation of nonlinear interpolation schemes. These characteristic functions for the interpolation operator are taken as follows:

$$f_i = \begin{cases} \sum_{k=1}^{N-1} z_k, & i = 1, \\ \frac{\sum_{k=i}^{N-1} z_k}{\sum_{k=i-1}^{N-1} z_k}, & i > 1. \end{cases} \quad (11)$$

If given initial values of volume fractions satisfy the condition (8), then the initial values of characteristic functions f_i are constrained by the following condition:

$$f_i^0 \in 0, 1, \quad x \in x_L, x_R, \quad i = 1, 2, \dots, N-1. \quad (12)$$

When monotonicity-preserving higher-order schemes are applied to f_i^0 , the interpolated values of f_i^0 at cell faces will also satisfy the condition (8),

$$f_{i,cf}^0 \in 0, 1, \quad x \in x_L, x_R, \quad i = 1, 2, \dots, N-1. \quad (13)$$

where the subscript “cf” indicates the interpolated values at cell faces.

Combing Eqs. (11) and (13), we obtain the following

$$\begin{cases} \sum_{k=1}^{N-1} z_{cf,k}^0 \in 0, 1, \\ \frac{\sum_{k=i}^{N-1} z_{cf,k}^0}{\sum_{k=i-1}^{N-1} z_{cf,k}^0} \in 0, 1, \quad i = 1, \dots, N-1, \end{cases} \quad (14)$$

which means

$$0 < z_{cf,N-1}^0 < \sum_{k=N-2}^{N-1} z_{cf,k}^0 < \dots < \sum_{k=2}^{N-1} z_{cf,k}^0 < \sum_{k=1}^{N-1} z_{cf,k}^0 < 1. \quad (15)$$

Comparison of inequality (15) with condition (10) shows that these constraints on volume fractions are equivalent. Thus, we obtain interpolated volume fractions at cell faces such that the constraints in (9) and (10) are valid.

Although the characteristic functions in the form of (11) ensure that the interpolated volume fractions satisfy the constraints in (9) and (10), they fail to maintain the desirable well-balancing property (keeping constant distributions in pressure and velocity). Similar to the work [12], one can show that to preserve constant pressure and velocity distributions (the

PV property), the advection functions $f_i(z_1, z_2, \dots, z_{N-1})$ must be linear with respect to z_j . In the present paper, we choose the following simple characteristic functions to update the volume fractions in time:

$$f_i = \sum_{k=i}^{N-1} z_k. \quad (16)$$

Therefore, we utilize two different sets of characteristic functions: characteristic functions (11) for the face interpolation operator and characteristic functions (16) for time step updating.

Since both cell averages and interpolated values of initial volume fractions are kept, the evolved cell averages of volume fractions after one time step will also satisfy the constraints in (9) and (10). By a recursive procedure, we deduce that the evolved cell averages of volume fractions in all the following time steps also will satisfy (9) and (10).

4 NUMERICAL RESULTS

In this section, we consider several 2D benchmark problems to examine the performance of our method. The approximate Riemann solver HLLC is utilized to calculate the inter-cell numerical flux and the explicit Euler scheme is used for time integration. For the high-order extension, we adopt the MUSCL scheme with the MINMOD limiter. The MUSCL scheme is applied to the characteristic function (11), and the characteristic functions (16) are then updated with time. The CFL number is set to be 0.2.

4.1 Passive transport of three materials

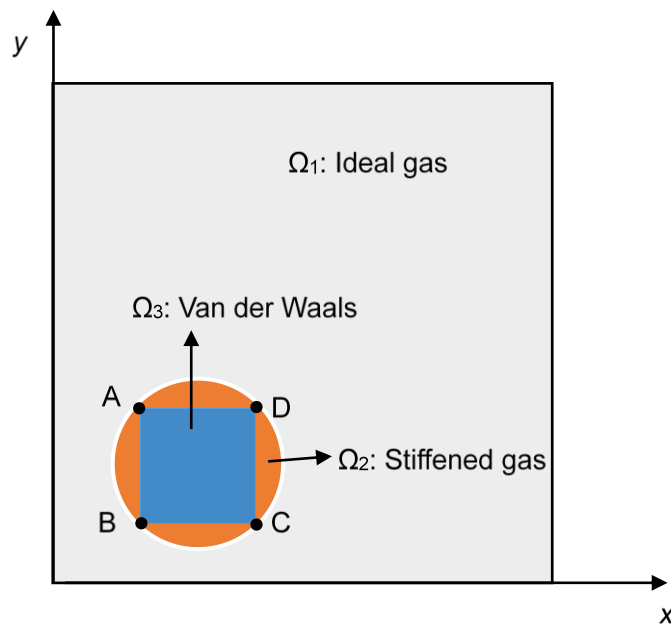


Figure 1: The passive transport problem statement.

As shown in Fig. 1, the computational domain is a square with edges 1.0m long. Three

materials are initially located in the domains Ω_1 , Ω_2 , Ω_3 , respectively. These materials are characterized by the ideal gas EOS, the stiffened gas EOS and the Van der Waals EOS, respectively. The parameters of the EOSs [14] are shown in Table 1.

Table 1: Material properties for the passive transport problem.

Material	γ	a (Pa·m ⁶ /kg)	b (m ³ /kg)	π (Pa)
Ideal gas	1.400	0	0	0
Stiffened gas	4.400	0	0	6.000×10^8
Van der Waals gas	1.300	5	10^{-3}	6.000×10^8

The center of the circle is initially located at the point (0.25m, 0.25m), and the radius of the circle is 0.20m. At the points A, B, C, three materials come into contact. Three materials are passively transported by the velocity $u = (1000 \text{ m/s}, 1000 \text{ m/s})$. Constant boundary conditions are imposed on the left and lower boundaries, and transmissive boundary conditions are imposed on the right and upper boundaries.

The initial conditions are given as

$$\begin{aligned}
 & \rho_1 \quad \rho_2 \quad \rho_3 \quad u \quad v \quad P \quad z_1 \quad z_2 \\
 & = \begin{cases} \left[1.29 \quad 10^3 \quad 50 \quad 10^3 \quad 10^3 \quad 10^5 \quad 1-10^{-6} \quad 5 \times 10^{-7} \right], x \in \Omega_1, \\ \left[1.29 \quad 10^3 \quad 50 \quad 10^3 \quad 10^3 \quad 10^5 \quad 5 \times 10^{-7} \quad 1-10^{-6} \right], x \in \Omega_2, \\ \left[1.29 \quad 10^3 \quad 50 \quad 10^3 \quad 10^3 \quad 10^5 \quad 5 \times 10^{-7} \quad 5 \times 10^{-7} \right], x \in \Omega_3, \end{cases} \quad (13)
 \end{aligned}$$

where z_1, z_2 stand for the volume fractions of the ideal gas material and the stiffened gas material, respectively.

After 500 μ s we obtain the numerical results shown in Fig. 2. It can be seen that the distribution of the materials are well maintained after advection. Some smearing of the material interface can be observed. This defect can be suppressed with various interface sharpening techniques. This issue will be tackled in a separate paper.

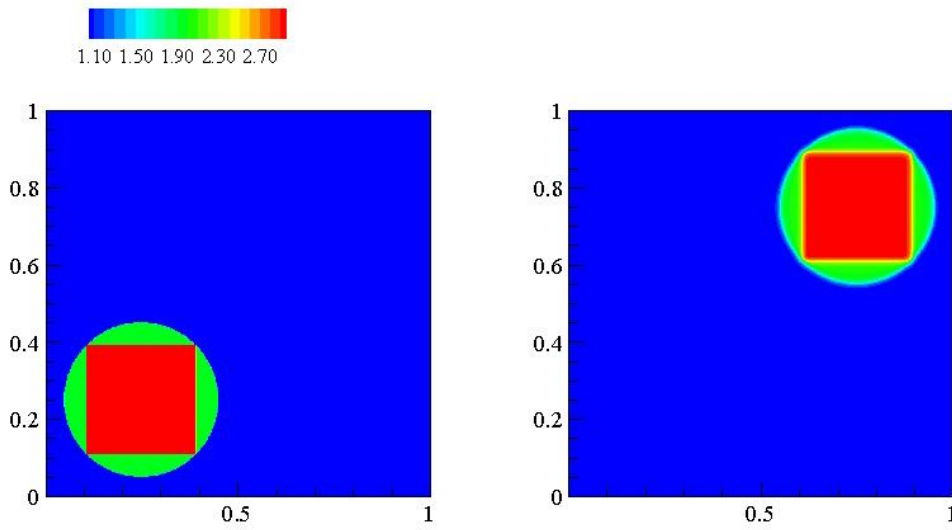


Figure 2: Distribution of the variable $Z = \sum_{k=1}^3 k z_k$.

To check the well-balancing property of the method, we also include the plots of the magnitude of errors in pressure and velocity in Fig. 3. We see that the difference between approximate and exact solutions are of the order 10^{-6} and 10^{-11} , respectively, which means that the pressure and velocity equilibrium is well maintained.

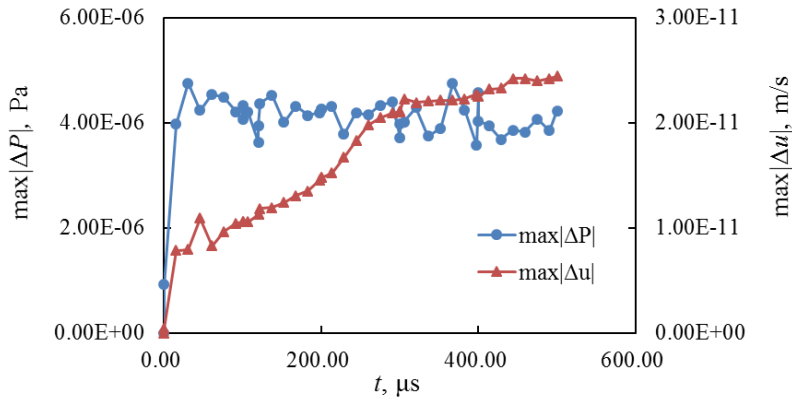


Figure 3: Evolution of maximum errors in pressure and velocity with time.

4.2 Richtmyer-Meshkov instability

This test is taken from [13]. The computational domain has a rectangular shape (see Fig. 4). The domain Ω_1 is filled with the dense gas SF_6 (sulphur hexafluoride), and the domain Ω_2 with air. The gases are in equilibrium at the beginning. A shock wave enters into the computational domain from the left boundary. On the other boundaries reflective boundary conditions are imposed. The shock wave travels through the SF_6 block, and then reflects on the right boundary. The leftward reflected shock wave hits the block again and travels through it. Due to the interaction with the shock wave, the SF_6 block loses its initial rectangular shape

and undergoes strong deformation.

Although the experiment in [13] only involves two domains and two materials, we will assume existence of a third domain Ω_3 on the left to the domain Ω_2 , as illustrated in Fig. 4. The domain Ω_3 is filled with a material whose thermodynamic parameters are identical with air and the state vector is the same as that assigned at the left boundary LB . This problem statement has no impact on the numerical results, since the left boundary condition remains unchanged. However, the problem in this case can be treated as a three-material problem.

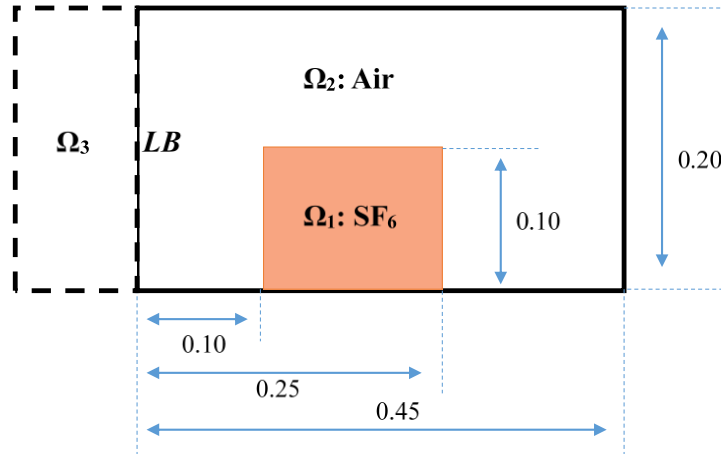


Figure 4: Configuration for the problem of shock/SF6 block simulations.

Both air and SF_6 are characterized as perfect gases with adiabatic coefficients $\gamma_{\text{air}}=1.400$ and $\gamma_{\text{SF}_6}=1.076$, respectively. The initial conditions are given as follows:

$$\begin{aligned}
 & \rho_1 \quad \rho_2 \quad \rho_3 \quad u \quad v \quad P \quad z_1 \quad z_2 \\
 & = \begin{cases} \left[1.667 \quad 5.805 \quad 1.153 \quad 0 \quad 0 \quad 96856.0 \quad 5 \times 10^{-7} \quad 1 - 10^{-6} \right], x \in \Omega_1, \\ \left[1.667 \quad 5.805 \quad 1.153 \quad 0 \quad 0 \quad 96856.0 \quad 5 \times 10^{-7} \quad 5 \times 10^{-7} \right], x \in \Omega_2, \\ \left[1.667 \quad 5.805 \quad 1.153 \quad 133.273 \quad 0 \quad 163256.0 \quad 1 - 10^{-6} \quad 5 \times 10^{-7} \right], x \in LB, \end{cases}
 \end{aligned}$$

where LB denotes the left boundary, and volume fractions z_1 and z_2 represent the fictitious material in domain Ω_3 and SF_6 , respectively.

The numerical results are compared with the experimental images in Fig. 5. A very good agreement can be observed. From the numerical Schlieren image in the third column, one can see the interaction between the shock and the SF_6 block, the transmission and reflection of the shock waves. We further provide a more close comparison between experimental images and numerical Schlieren images in Fig. 6. The x - and y -extent distributions of the SF_6 block are in good agreement with the experimental results. Moreover, the distribution of volume fraction z_1 and z_2 are displayed in Fig. 7 and Fig. 8, respectively.

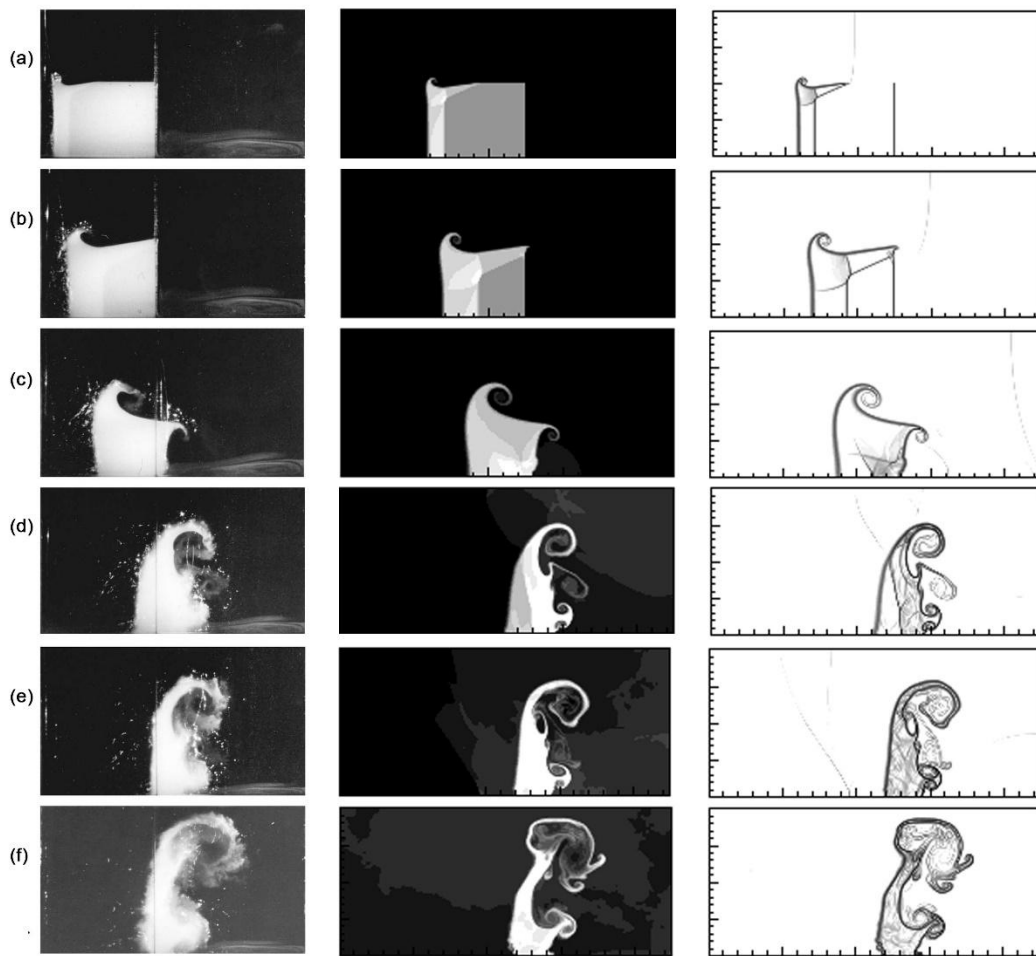


Figure 5: Comparison between experimental images (left column: laser-sheet frames) and numerically generated images (second column: density distribution, third column: numerical Schlieren image). Times displayed are (a) 206, (b)446, (c)926, (d)1726, (e)2046, (f)2846 μ s.

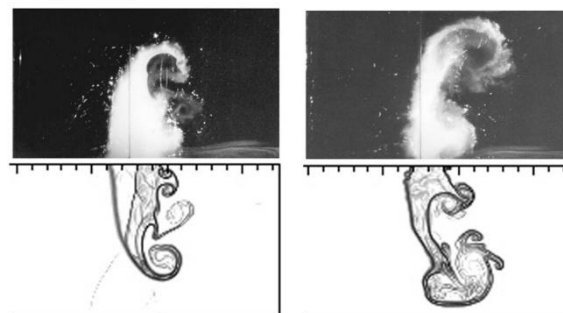


Figure 6: Comparison between experimental images and numerical Schlieren images at two times (d)1726 and (f)2846 μ s

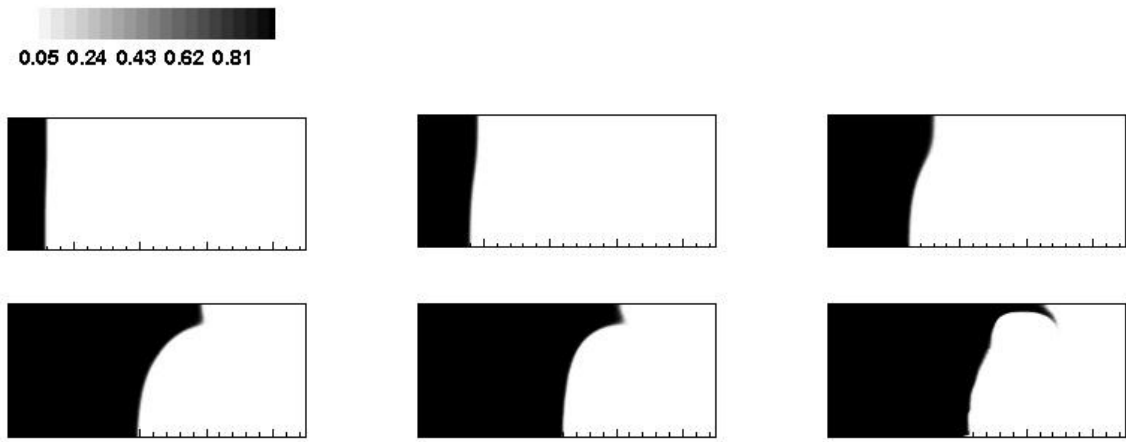


Figure 7: Evolution of the volume fraction z_1 .

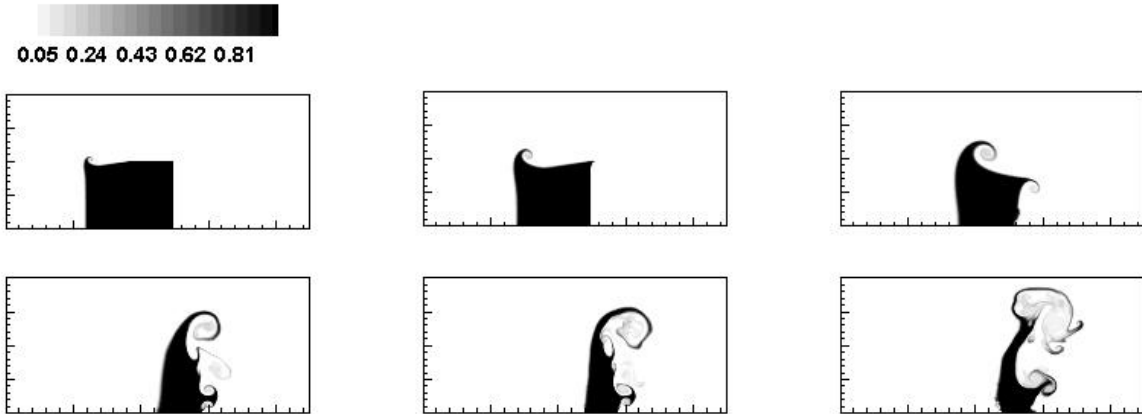


Figure 8: Evolution of the volume fraction z_2 .

5 CONCLUSIONS

A numerical approach have been considered for modeling heterogeneous media composed of multiple compressible materials with different physical properties. The physical model was based on the single-velocity assumption, and the governing equations represent mass conservation for each component, conservation of the total momentum and energy, and advection of $N-1$ characteristic functions that depend on volume fractions of N components. The isobaric assumption was used to close the model equations. Main inferences that can be made from this study are as follows.

- Special advection functions for updating and special advection functions for reconstruction of volume fractions have been suggested, for which higher-order schemes and sharpening techniques can be implemented without introducing spurious oscillations in numerical solutions and violation of the well-balancing property of the scheme.

- Numerical results demonstrate the efficiency and accuracy of the proposed numerical method and computational algorithm.
- The future work can be seen related to the development of the considered method by adding the phase transition process and engineering applications.

Acknowledgements The first author thanks the China Scholarship Council for their financial support. The reported study was partially supported by RFBR, research project No. 18-01-00921.

REFERENCES

- [1] Hirt, C.W. , Nichols B.D. Volume of fluid (VOF) method for the dynamics of free boundaries. *Journal of Computational Physics* (1981) **39**(1):201-225.
- [2] Dyadechko, V. , Shashkov, M. Reconstruction of multi-material interfaces from moment data, *J. Comput. Phys.* (2008) **227**:5361-5384.
- [3] Luo, H., Baum, J.D., Lohner, R. On the computation of multi-material flows using ALE formulation. *J. Comput. Phys.* (2004) **194**:304-328.
- [4] Terashima, H., Tryggvason, G. A front-tracking/ghost-fluid method for fluid interfaces in compressible flows. *J. Comput. Phys.* (2009) **228**:4012-4037.
- [5] Osher, S. , Fedkiw, R.. *Level sets and dynamic implicit surfaces*. Springer-Verlag: New York, 2002.
- [6] Fedkiw, R., Aslam, T., Merriman, B. , Osher S. A non-oscillatory Eulerian approach to interfaces in multimaterial flows (the ghost fluid method). *J. Comput. Phys.* (1999) **152**:457-492.
- [7] Shyue, K.M. An efficient shock-capturing algorithm for compressible multicomponent problems, *J. Comput. Phys.* (1998) **142**:208-242.
- [8] Saurel, R. , Abgrall, R. A simple method for compressible multifluid flows, *SIAM J. Sci. Comput.* (1999) **21**:1115-1145.
- [9] Allaire, G., Clerc, S., Kokh, S. A five-equation model for the simulation of interfaces between compressible fluids. *J. Comput. Phys.* (2002) **181**:577-616.
- [10] Friessa, M.B., Kokh, S. Simulation of sharp interface multi-material flows involving an arbitrary number of components through an extended five-equation model. *J. Comput. Phys.* (2014) **273**:488-519.
- [11] Jaouen, S., Lagoutière, F. Numerical transport of an arbitrary number of components. *Comput. Methods Appl. Math.* (2007) **196**(33-34):3127-3140.
- [12] Zhang, C., Menshov, I. An Eulerian Model for Simulation of Multi-fluid Flows with Interfaces, MSU Moscow, unpublished work.
- [13] Bates, K.R., Nikiforakis, N., Holder, D. Richtmyer-Meshkov instability induced by the interaction of a shock wave with a rectangular block of SF₆. *Physics of Fluids* (2007) **19**: 036101.
- [14] Shyue, K.M. A fluid-mixture type algorithm for compressible multicomponent flow with van der Waals equation of state. *J. Comput. Phys.* (1999) **156**:43-88.
- [15] Batten, P., Clarke, N., Lambert, C., Causon, D.M. On the choice of wavespeeds for the HLLC Riemann solver. *SIAM J. Sci. Comput.* (1997) **18**:1553-1570.
- [16] Olsson, E., Kreiss, G., Zahedi, S. A conservative level set method for two phase flow, II. *J. Comput. Phys.* (2007) **225**:785-807.